scientific reports

Check for updates

OPEN

Biomechanical effects of LCWHTO vs. MOWHTO on medial meniscus posterior root repair: a finite element analysis

Fan Yang[1,2], Takuji Yokoe[1]✉, Koki Ouchi[1], Takuya Tajima[1], Naosuke Kamei[1] & Etsuo Chosa[1]

Whether isolated high tibial osteotomy (HTO) or HTO combined with medial meniscus posterior root (MMPR) repair is the optimal surgical treatment of MMPR tears remains controversial. This study compared the biomechanical effects of isolated HTO versus MMPR repair combined with medial open wedge HTO (MOWHTO) or lateral closed wedge HTO (LCWHTO) using finite element analysis (FEA). In this study, the MRI and CT data of the knee joint were used to create an FEA model. MOWHTO and LCWHTO simulations adjusted the mechanical axis to the Fujisawa point, with MMPR conditions simulated as intact, tear, or repaired. The ankle center was fixed and a 1000 N force was applied to the knee. In the LCWHTO models, the posterior tibial slope (PTS) decreased, whereas it increased in the MOWHTO models. Changes in the PTS following HTO influenced the stress distribution in the MMPR. HTO combined with MMPR repair showed a reduction in the maximum contact stress by 5.4–11.4% and increased contact area by 29.5–41.0% in the medial knee compartment relative to isolated HTO. This study demonstrated that MMPR repair combined with LCWHTO would be more protective against stress loading in the MMPR than MMPR repair combined with MOWHTO or isolated HTO.

Medial meniscus posterior root (MMPR) tear (MMPRT) is not an uncommon meniscal injury, representing 10.1–27.8% of all meniscal tears[1,2]. MMPRT has been reported to be associated with increased tibiofemoral stress in the medial knee compartment[3]. Consequently, the medial meniscus and the articular cartilage tend to undergo accelerated degeneration[4–6]. MMPRTs is also significantly influenced by varus knee alignment[1,7]. Recent clinical studies have highlighted that delayed surgical treatment for MMPRT accelerates the progression of osteoarthritis[6,8,9].

In terms of treatment strategies for MMPRTs, several studies have advocated not only MMPR repair but also high tibial osteotomy (HTO), either alone or in combination with MMPR repair[10–12]. These combined surgical techniques demonstrated significant clinical improvements in MMPRT healing and medial cartilage regeneration[13,14]. However, second-look arthroscopic examinations have revealed incomplete healing of the MMPR after MMPR repair combined with HTO[10,14,15]. Therefore, there is still room for improvement in surgical strategies for MMPRTs. Recent imaging studies indicate that medial opening wedge high tibial osteotomy (MOWHTO) generally increases the posterior tibial slope (PTS), while lateral closing wedge high tibial osteotomy (LCWHTO) tends to decrease PTS[16–18]. A steeper PTS has been reported to be a significant risk factor for MMPRTs[19,20]. However, as far as we know, no studies have evaluated the influence of MOWHTO vs. LCWHTO on stress distribution in the MMPR. In addition, it remains controversial whether isolated MMPR repair or MMPR repair combined with HTO is more protective against stress distribution in the MMPR. The purpose of this study was to investigate the biomechanical effects of isolated HTO compared to MMPR repair combined with HTO on the MMPR. The present study hypothesized that combining MMPR repair with HTO would be more protective against MMPR than isolated HTO or isolated MMPR repair. Additionally, this study hypothesized that MMPR repair combined with LCWHTO would be preferable in terms of biomechanical status in the MMPR in comparison to MMPR repair combined with MOWHTO.

[1]Division of Orthopaedic Surgery, Department of Medicine of Sensory and Motor Organs, Faculty of Medicine, University of Miyazaki, 5200 Kihara, Kiyotake 889-1692, Miyazaki, Japan. [2]Department of Orthopaedics Surgery, Qinghai University Affiliated Hospital, Xining 810000, Qinghai, China. ✉email: yokoetakuji@gmail.com

Results

Change in the PTS following HTO

As illustrated in Fig. 1(a), following HTO, each model exhibited distinct alterations in the PTS relative to the native knee model. The PTS in the LCWHTO (90) and MOWHTO (90) models did not change relative to the native knee model. The PTS in the LCWHTO (30) and LCWHTO (60) models reduced by 3.1° and 1.0°, respectively, compared to the native knee model. In contrast, the PTS in the MOWHTO (30) and MOWHTO (60) models increased by 3.1° and 1.0°, respectively, relative to the native knee model.

Maximum von mises stress and shear stress in the MMPR

The von Mises stress (VMS) and shear stress in the MMPR for each model are shown in Figs. 1(a) and 2. In the native knee model, the maximum VMS and shear stress were 26.0 MPa and 14.3 MPa, respectively. The LCWHTO (90) and MOWHTO (90) models exhibited comparable stress distributions in the MMPR. In the LCWHTO models, the maximum VMS and shear stress in the MMPR reduced by 3.8-33.1% and 3.4-26.5%, respectively, compared to the native knee model. Conversely, in the MOWHTO models, the maximum VMS and shear stress in the MMPR increased by 10.9-46.5% and 11.5-45.0%, respectively, compared to the native knee model.

Contact stress in the medial knee compartment

The distribution of contact stress in the medial knee compartment is illustrated in Figs. 1(b) and 3. In all models, the LCWHTO (90) and MOWHTO (90) models exhibited comparable contact stress distributions in the medial knee compartment. Compared to the MOWHTO (90) model, the MOWHTO (30) model showed increased contact stress. Conversely, the LCWHTO (30) model demonstrated reduced contact stress relative to the LCWHTO (90) model.

Figure 1(c) shows that MMPR repair combined with HTO reduces contact stress in the medial knee compartment relative to isolated HTO, with an average decrease of 8.3% in the MTC and 8.6% in the MFC.

Contact area in the medial knee compartment

As shown in Fig. 3, each model demonstrated variations in contact area under identical loading and boundary conditions. Specifically, in the LCWHTO (30) model, the contact area increased by an average of 37.8% in the MTC, 32.8% in the MM, and 24.7% in the MFC relative to the MOWHTO (30) model. Isolated HTO resulted in a smaller contact area in the medial knee compartment relative to MMPR repair combined with HTO, with an average decrease of 6.7% in the MTC and 37.5% in the MFC.

Discussion

The most significant findings of this study are as follows: (1) MMPR repair combined with HTO is biomechanically advantageous over isolated HTO for the treatment of MMPRT; (2) MMPR repair combined with LCWHTO provided better protection against shear stress and contact stress in the MMPR in comparison to MMPR repair combined with MOWHTO. The study findings revealed that MOWHTO tends to increase PTS, while LCWHTO tends to decrease it. An increase in PTS can lead to elevated shear stress and VMS in the MMPR, potentially compromising the integrity of MMPR repair or delaying the healing process. Additionally, increased PTS was associated with heightened contact stress and reduced contact area in the medial knee compartment, which may negatively affect surgical outcomes and accelerate OA progression. These findings support the hypothesis of the current study, highlighting the importance of adjustment of the PTS for obtaining better clinical outcomes following surgery of the MMPRT.

Isolated HTO vs. MMPR repair combined with HTO

When comparing isolated HTO with MMPR repair combined with HTO, the combined approach significantly reduced contact stress and increased the contact area in the medial knee compartment in the present study. This biomechanical advantage may be crucial for protecting the cartilage in the medial knee compartment from excessive stress and for promoting MMPR healing[8]. Several studies have supported the superiority of the combined surgical strategy, demonstrating a higher MMPR healing rate in patients treated with MMPR repair combined with HTO in comparison to those treated with isolated HTO[10,15]. The present study similarly revealed that MMPR repair combined with HTO reduced the maximum contact stress in the medial knee compartment by 5.4–11.4%, while the contact area increased by 29.5–41.0%. In addition to reducing the contact stress in the medial knee compartment, MMPR repair combined with HTO may also help restore the hoop stress of the meniscus. Many studies have demonstrated that isolated HTO is insufficient to address medial meniscal extrusion (MME), a critical pathological condition associated with meniscal dysfunction[12].

Some authors have reported superior postoperative outcomes in patients who underwent MMPR repair combined with MOWHTO in comparison to those treated with isolated MOWHTO. Lan et al. reported an 85.7% healing rate in a group that received MMPR repair combined with MOWHTO, whereas the healing rate in their isolated HTO group was only 45.4% [10]. Furthermore, Choi et al., in a retrospective study, found that MMPR repair combined with MOWHTO significantly enhanced MMPR healing rates and promoted cartilage regeneration in MFC[14]. Despite the advantages of the combined approach, incomplete healing of MMPR still requires attention. According to a study by Jing et al., a second-look arthroscopic evaluation revealed that 59% of patients who underwent the combined approach exhibited partial healing of the MMPR[15]. This could be partially attributed to the increased PTS following MOWHTO, which results in greater stress on the MMPR[21,22].

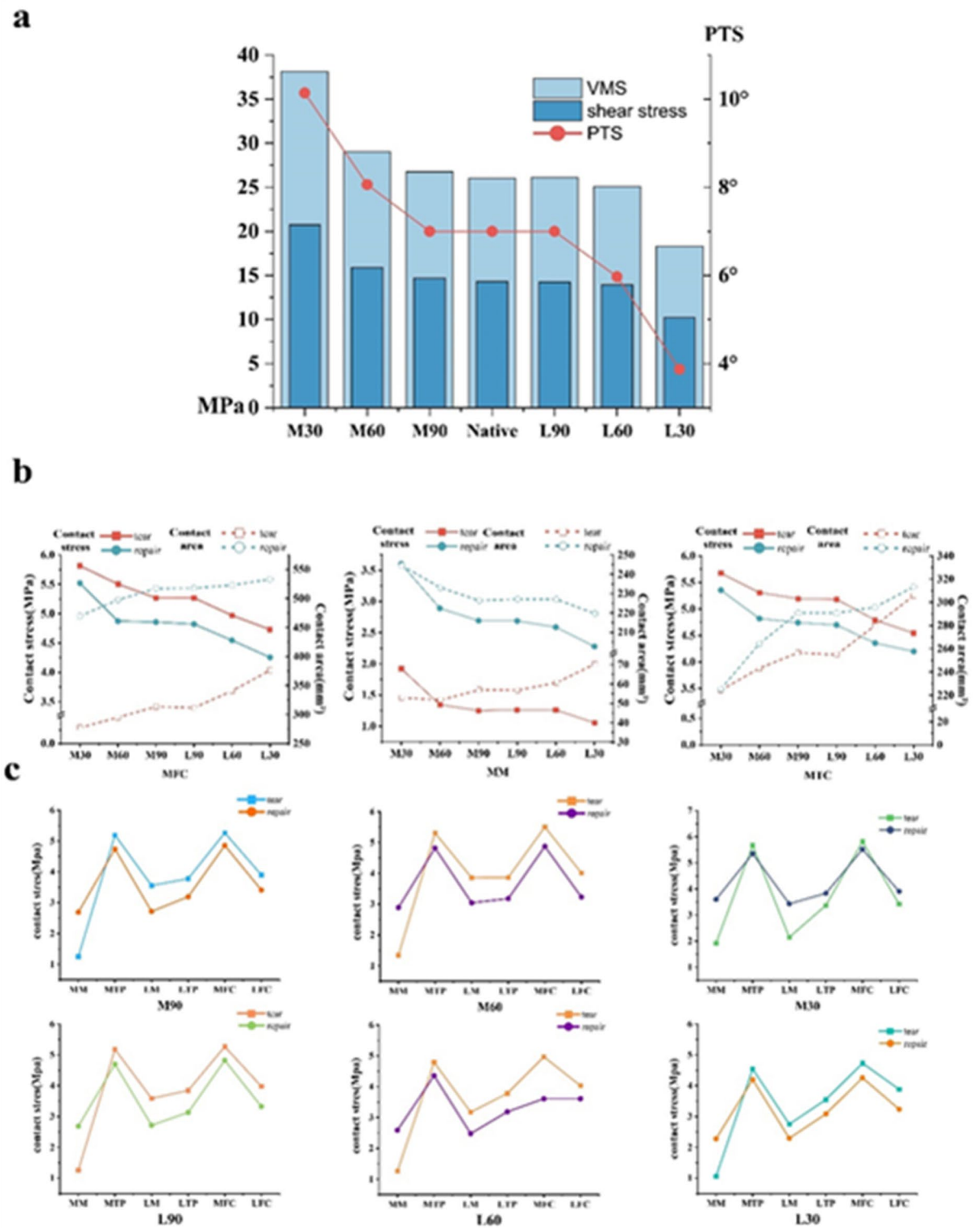

Fig. 1. Influence of the method of high tibial osteotomy and the status of the medial meniscus posterior root on stress distribution in the medial meniscus posterior root or on each component of the knee joint. (**a**) The relationship between the posterior tibial slope and von Mises stress and shear stress in the medial meniscus posterior root after each high tibial osteotomy. (**b**) Contact stress and contact area in the medial knee compartment for each method of high tibial osteotomy and the status of the medial meniscus posterior root. (**c**) Contact stress in each component of the knee joint for each method of high tibial osteotomy and the status of the medial meniscus posterior root. *PTS* posterior tibial slope, *VMS* von Mises stress, *MFC* medial femoral condyle, *MM* medial meniscus, *MTP* medial tibial plateau, *LFC* lateral femoral condyle, *LM* lateral meniscus, *LTP* lateral tibial plateau.

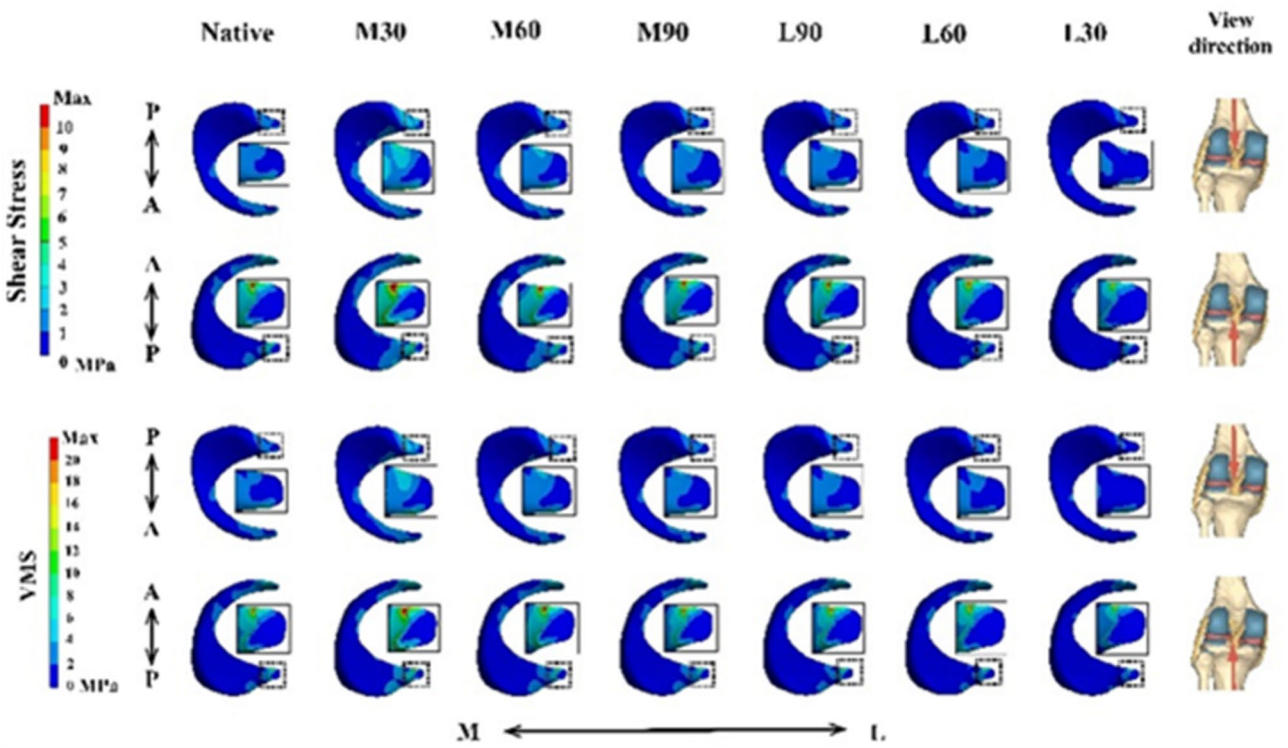

Fig. 2. Shear stress and von Mises stress (VMS) in the medial meniscus posterior root under each method of high tibial osteotomy. *A* anterior, *P* posterior, *M* medial, *L* lateral.

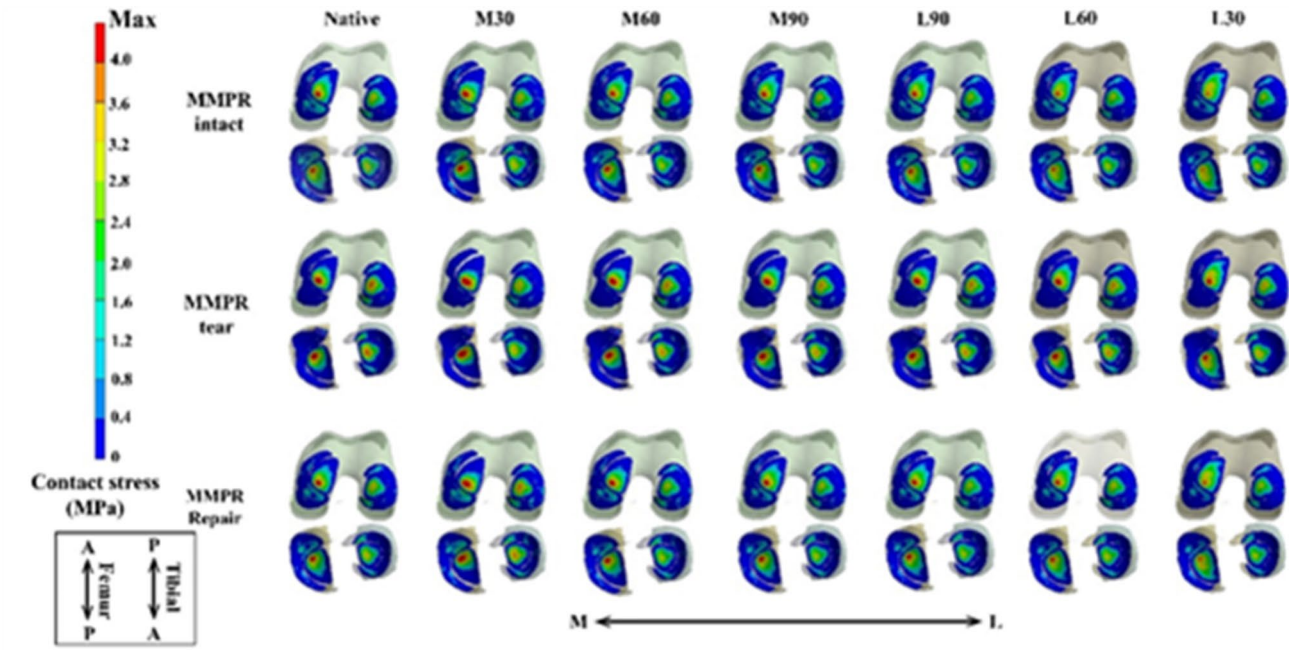

Fig. 3. Stress distribution in the knee joint under each method of high tibial osteotomy. *MMPR* medial meniscus posterior root, *A* anterior, *P* posterior, *M* medial, *L* lateral.

MMPR repair combination with LCWHTO vs. MOWHTO

This study examined the biomechanical differences between MMPR repair combined with MOWHTO and LCWHTO. It has been shown that MOWHTO generally increases PTS, whereas LCWHTO tends to reduce it[16,17]. The present study observed alterations in the PTS following each HTO technique. The present study findings further demonstrated that the direction of osteotomy may have a different effect on the PTS regardless of whether MOWHTO or LCWHTO is performed. This is consistent with the findings of LaPrade et al., who found that anteromedially placed plates resulted in steeper PTS in comparison to posteromedially placed plates[21].

In this study, increased PTS following MOWHTO led to increased shear stress and VMS in the MMPR, with shear stress and VMS increasing by 10.9–46.5% and 11.5–45.0%, respectively. This can be attributed to the posterior rollback of the femoral condyle and anterior translation of the tibia[22], which results in elevated stress in the MMPR. Such increased stress is associated with delayed or hindered MMPR healing[23,24]. In contrast, LCWHTO, which reduces PTS, led to a decrease in shear stress and VMS in the MMPR by 3.8–33.1% and 3.4–26.5%, respectively. Based on the findings of this study, LCWHTO may offer a more favorable biomechanical environment for MMPR healing, making it a preferable surgical technique when combined with MMPR repair[23,24]. Therefore, optimizing the postoperative PTS during MMPR repair combined with HTO may represent a promising surgical approach. Further clinical studies are required to verify this hypothesis.

Notably, similar biomechanical behaviors were observed in the medial knee compartment across the native, LCWHTO (90), and MOWHTO (90) models when the PTS was maintained at the same value. This consistency can be attributed to the minimal adjustment of the coronal mechanical axis in all HTO models to a standardized angle, effectively reducing the impact of coronal alignment variations on medial knee biomechanics. Consequently, the primary factor influencing the medial knee biomechanics in this study was the change in the PTS following HTO. A further analysis demonstrated that the more anterior the osteotomy position in LCWHTO, the smaller the resulting PTS. This reduction in PTS is associated with an increased contact area and reduced contact stress in the medial knee compartment, promoting cartilage regeneration and preserving the meniscal function[3,19]. In contrast, MOWHTO, with a more anterior osteotomy position, led to a greater postoperative PTS than LCWHTO, which resulted in increased contact stress and a reduced contact area in the medial knee compartment. These biomechanical changes may result in a less favorable environment for the medial knee compartment. The postoperative increase in PTS following MOWHTO may be due to the osteotomy site being more anterior and closer to the pes anserinus[21,25]. The increased PTS after MOWHTO contributes to the suboptimal outcomes reported in MMPR repair combined with MOWHTO[23,24]. Based on the findings of the current study, in preoperative planning, careful consideration should be given to the osteotomy site and direction, as these factors directly influence the postoperative PTS and stress distribution in the MMPR. Osteotomy performed at a more anterior and lateral site during LCWHTO generally results in a decreased PTS and more favorable stress distribution in the medial knee compartment and MMPR. The influence of this surgical strategy on clinical outcomes, especially the healing status of MMPR, needs to be investigated in future clinical studies. Maintaining the PTS during HTO remains a key focus in some clinical and biomechanical studies. Some authors have introduced techniques to mitigate the increase of PTS following MOWHTO, such as asymmetric gap of the osteotomy, modification to the anterior and posterior hinge positions, and optimized fixation methods[26–29]. These approaches are particularly relevant in cases where excessive PTS contributes to knee instability, especially in patients with concurrent anterior cruciate ligament or posterior cruciate ligament injuries.

The current study primarily investigated the biomechanical impacts of HTO on MMPRT, and focused on the variations in osteotomy angle and direction while excluding anterior-posterior osteotomy gap asymmetry as a variable. However, given the irregular quadrilateral geometry of the proximal tibia, some degrees of variation in the anterior and posterior osteotomy gaps were unavoidable. Future studies will be needed to evaluate the biomechanical effects of adjustments of the osteotomy gap on knee biomechanics. Such investigations could provide further insights into surgical strategies to control PTS at the time of surgery of the MMPRT.

Limitations

This study has several limitations. First, the study data were obtained from a single healthy volunteer, which may restrict the generalizability of the study findings to patients with different knee alignments. Second, the knee models only considered the essential bone and soft tissues of the knee joint, which simplifies the HTO procedure. In clinical practice, variations in surgical techniques and the release of the posterior soft tissue may influence postoperative PTS. Third, although a standardized double-suture technique was used for MMPR repair in this study, different suture techniques could result in different outcomes. Fourth, this study focused on biomechanical changes in the extended knee joint and did not evaluate the stress distribution in the MMPR at different knee flexion angles[30]. Further studies are needed to investigate the biomechanical alterations at different flexion angles of the knee joint. Finally, the material properties in the FEA were based on standard data, but individual variations in the knee components affected the results. Additionally, the use of von Mises stress, which assumes isotropic material behavior, may not fully represent the anisotropic nature of the meniscus, which affected the analysis of stress distribution. Despite these limitations, this is the first study to evaluate the differences in stress distribution in the MMPR between isolated HTO and MMPR repair combined with MOWHTO or LCWHTO.

Conclusions

This study demonstrated that LCWHTO and MOWHTO have distinct effects on the VMS and shear stress in the MMPR, primarily because of the changes in the PTS following each osteotomy technique. MMPR repair combined with HTO offered greater protection against knee joint contact stress than isolated HTO. Specifically, the combination of MMPR repair with LCWHTO improved the biomechanical environment of the tibiofemoral

joint and MMPR, suggesting its potential superiority to MMPR repair combined with MOWHTO as a surgical procedure for MMPR tears.

Materials and methods

This study was approved by our institutional review board (Approval No. O-1488). All procedures adhered to the ethical standards outlined by the responsible committee on human experimentation and complied with the 1975 Declaration of Helsinki, as revised in 2013. Informed consent was obtained from the participant.

Data acquisition

In this study, a healthy 32-year-old male volunteer without a history of knee injury (Height, 180 cm; weight, 90 kg; BMI, 27.8) was enrolled. Computed tomography (CT) was performed using a high-resolution CT scanner (Canon Aquilion One, Tochigi, Japan). CT scans of the lower extremities were taken with the participant in the supine position with bilateral knee joints in full extension, with a slice thickness of 1.0 mm and a field of view of 500 mm. Additionally, magnetic resonance imaging (MRI) of the left knee joint in full extension was conducted using a 3-Tesla MR scanner (Siemens MAGNETOM Verio, Munich, Germany). The MRI protocol included a proton density-weighted sequence with the following parameters: number of excitations = 1, echo train length = 80, slice thickness = 0.8 mm, slice spacing = 0.8 mm, matrix = 192 × 192, and field of view = 154 mm. Specifically, the imaging parameters for the proton density-weighted sequence were set at a repetition time of 1200 ms and an echo time of 17 ms.

Three-dimensional (3D) reconstruction of the knee joint and FEA modeling

The CT data obtained from the left lower extremity were processed using the MIMICS software (version 24.0; Materialise, Leuven, Belgium) to generate detailed models of the femur, tibia, and fibula. MRI data from the left knee joint were used to extract anatomical structures of the soft tissue, including the femoral and tibial cartilage, medial and lateral menisci, anterior cruciate ligament (ACL), posterior cruciate ligament (PCL), medial collateral ligament (MCL), and lateral collateral ligament (LCL). The entire extraction process was conducted by a senior orthopaedic surgeon. Thereafter, the extracted data underwent Boolean operations and were imported into the 3-Matic software program (version 16.0; Materialise, Leuven, Belgium). CT scans of the left lower extremity were meticulously integrated with the soft tissue components of the knee joint obtained from MRI. This integration was achieved by precisely aligning the models using the bony landmarks of the knee joint. The goal of this process was to reconstruct a comprehensive 3D model of the lower extremity and knee joint.

Model generation and establishment of 3D coordinates

The fully assembled stereolithography (STL) format 3D model was imported from 3-Matic into a computer-aided design (CAD) software program (SolidWorks 2015, Dassault Systèmes, Paris, France). In the CAD software program, the coronal and sagittal planes were used to locate the line connecting the femoral head center and ankle joint center, representing the 3D mechanical axis of the lower limb, as shown in Fig. 4(a, d)[31]. In this study, the intersection point of the mechanical axis in the coronal plane and tibial plateau was recorded. The total width of the tibial joint surface was marked as a percentage, with the medial edge designated as 0% and the lateral edge as 100% [32]. The coronal plane mechanical axis of the model passed through the knee joint and was positioned at 54%, as illustrated in Fig. 4(b, c). A 3D coordinate system was established based on the mechanical axis, with the mechanical axis defined as the Z-axis. The Y-axis represented the medial-lateral direction on the coronal plane, perpendicular to the mechanical axis, and the X-axis was defined as the anterior-posterior direction, perpendicular to the coronal plane. Using this 3D coordinate system as a reference, subsequent 3D coordinate systems for each HTO model were established, as illustrated in Fig. 5(a).

Surgical simulation of the HTO

The hinge point of the osteotomy was determined according to a study by Teng et al.[28]. The coronal plane hinge point for MOWHTO was determined to be 5 mm medial to the lateral cortex of the femur at the level similar to the apex of the fibular head. Then, an anatomical axis of the tibia on the sagittal plane was drawn, and the 3D hinge point was determined as shown in Figs. 4 and 5[33]. Similarly, the 3D hinge point for LCWHTO was identified. The coronal plane hinge point was determined to be 5 mm lateral to the medial cortex of the femur at the same level as the apex of the fibular head[28]. Then, an anatomical axis of the tibia on the sagittal plane was drawn, and the 3D hinge point was determined as shown in Figs. 4 and 5.

Best-fit circles were drawn on the lateral and medial tibial plateaus, and the centers of the medial and lateral tibial plateaus were determined. The midpoint of the line connecting the two centers was defined as the center of the tibial plateau, as illustrated in Fig. 5. A planar coordinate system was established with the center of the tibial plateau as the origin. The horizontal axis represents the longest line segment between the medial and lateral cortical bones, while the vertical axis is in the anteroposterior direction perpendicular to the horizontal axis. Osteotomy points were determined based on the direction and angle of the coordinate system, as shown in Fig. 5.

The most commonly used surgical approach for HTO involves anterior osteotomy; therefore, an anterior approach was used. In this study, six different HTO angles were simulated as shown in Fig. 5: MOWHTO (30), MOWHTO (60), MOWHTO (90), LCWHTO (30), LCWHTO (60), and LCWHTO (90). The entry point of the osteotomy was located 40 mm distal to the knee joint, parallel to the tibial plateau, and perpendicular to the coronal plane[34]. A line connecting the osteotomy and projection points of the tibial plateau center on the hinge plane was established. On the hinge plane, a line perpendicular to this connecting line passing through the 3D hinge point was identified as the hinge axis corresponding to the osteotomy point (Fig. 5(c)). Based on

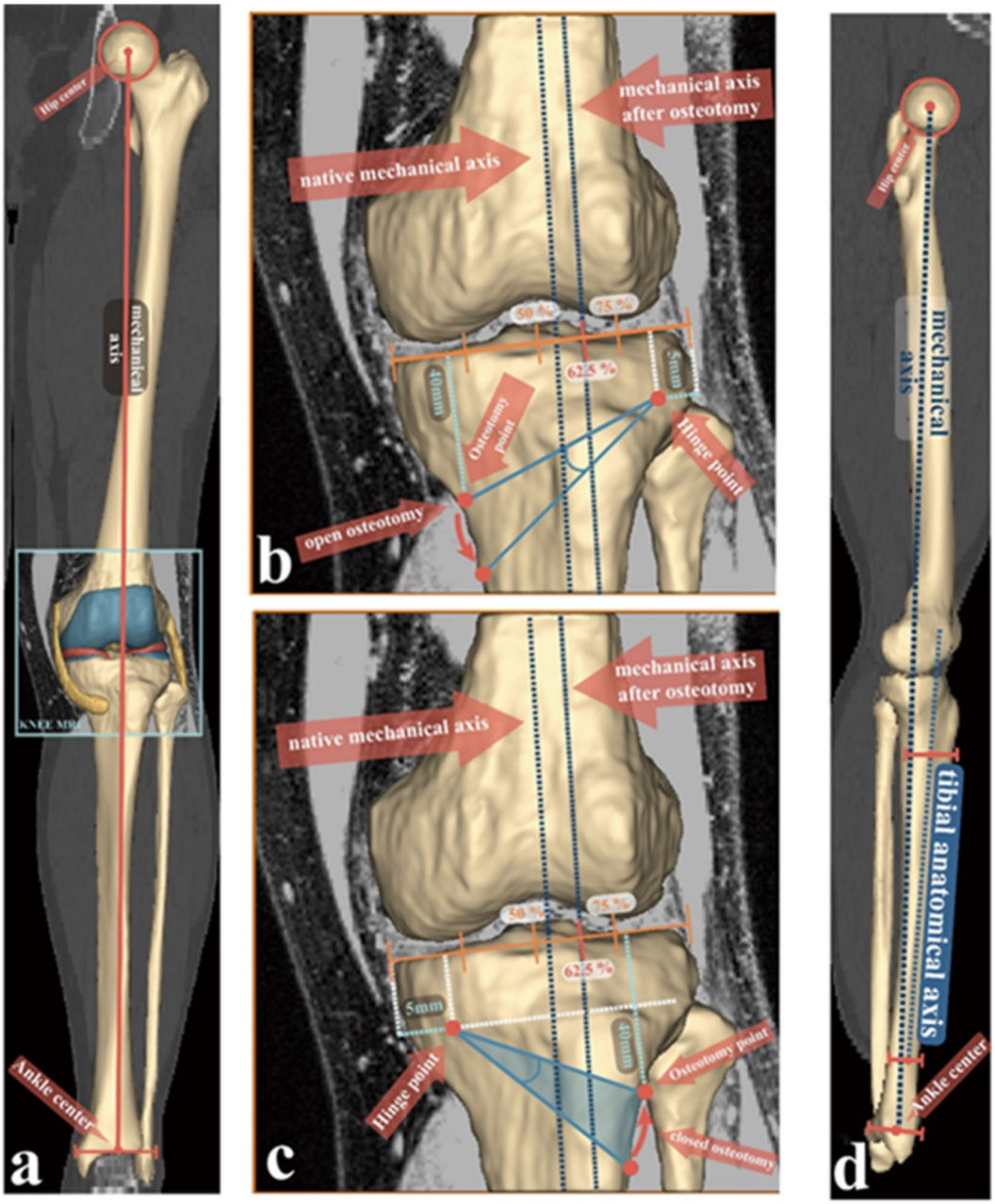

Fig. 4. Simulation of high tibial osteotomy (HTO). (**a**) Definition of the mechanical axis of the lower extremity. (**b**) Simulation of the medial open wedge HTO. The mechanical axis was planned to shift to the Fujisawa point (62.5% from the medial to the lateral side of the tibial plateau) following osteotomy. (**c**) Simulation of lateral closing wedge HTO. The mechanical axis was planned to shift to the Fujisawa point (62.5% from the medial to the lateral side of the tibial plateau) following osteotomy. (**d**) Sagittal view of the lower extremity showing the mechanical axis, tibial anatomical axis and posterior tibial slope (PTS).

the osteotomy points and their corresponding hinge axis, HTO angles with different osteotomy directions were created[35].

The goal of each HTO model was to change the mechanical axis of the lower extremity to the Fujisawa point, which is located at 62.5% from the medial to the lateral side of the tibial plateau[32]. All HTO models were corrected with 1.8° osteotomy in the coronal plane. PTSs before and after HTO were measured using the sagittal anatomical axis based on full-length 3D tibial models, as shown in Fig. 5(d)[36].

Medial meniscus posterior root tear and repair

According to the clinical definition, the region within 10 mm of the attachment site of the posterior horn of the medial meniscus is referred to as MMPR[37]. In this study, the MMPRT model was created as a meniscal injury 7 mm from the attachment site of the posterior horn of the medial meniscus. To simulate MMPR repair,

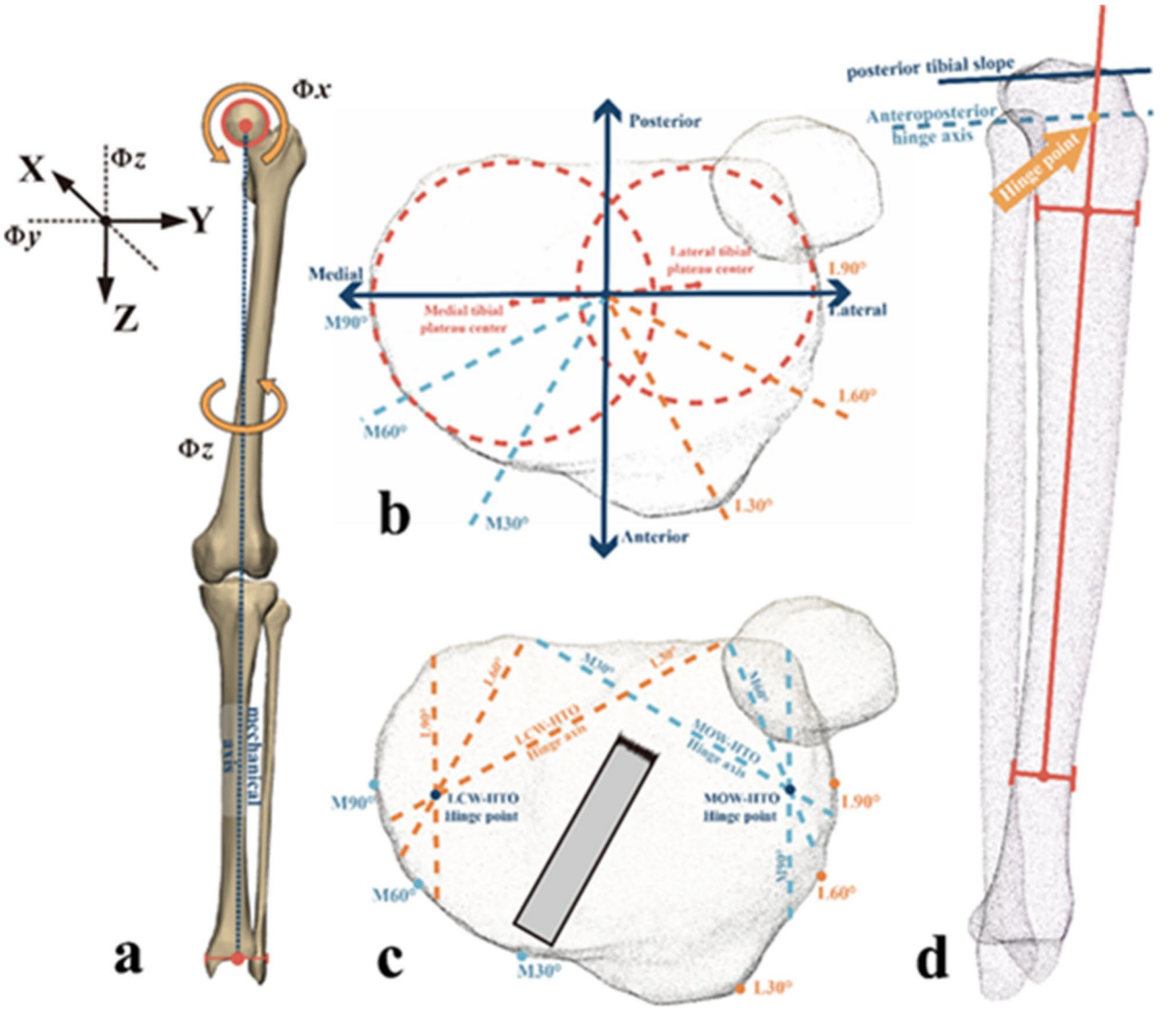

Fig. 5. Determination of 3D coordinate axes and simulation of high tibial osteotomy. (**a**) 3D coordinate axis of the lower extremity. (**b**) Determination of the center of the tibial plateau and osteotomy points. A total of six directions of high tibial osteotomy were simulated (MOWHTO30°, MOWHTO60°, MOWHTO90°, LCWHTO30°, LCWHTO60°, LCWHTO90°). (**c**) A sample of simulation of high tibial osteotomy (MOWHTO30°). (**d**) Determination of the 3D hinge point and posterior tibial slope.

the original tibial footprint of the MMPR was referenced, and the double-suture technique was applied to the MMPR according to a study by Steineman et al.[38]. During the MMPR repair simulation, two selected surfaces were connected by two tension-only spring components, each 7 mm in length with an average stiffness of 45 N/mm[39].

Material properties

After creating each model in SolidWorks software, they were imported into 3-Matic software (Materialise) for mesh generation. The models were then saved as STL format surface mesh files. Subsequently, these models were exported as STL files and imported into ANSYS Workbench (version 2024R1, ANSYS, Pennsylvania, USA) for a finite element analysis (FEA). Once the models were established in ANSYS Workbench, the material properties were assigned based on data from the relevant scientific literature. The bone components around the knee joint (femur, tibia, and fibula) were modeled using a linear isotropic elastic material model. The other bone models outside the knee joint were modeled using a simplified rigid-body material model. Correspondingly, the joint cartilage (femoral cartilage and medial and lateral tibial cartilage) and menisci were defined as linear isotropic elastic materials[40].

In this experiment, the ligaments (ACL, PCL, MCL, and LCL) were modeled as Neo-Hookean materials. Their constitutive model was identified as a nonlinear, incompressible, hyperelastic material with transverse isotropy. The strain energy function ψ of the hyperelastic material in the present study was as follows:

Tissue	Material model	Parameter	References
Bone	Linear elastic	E = 7300 MPa, ν = 0.3	40
Cartilage	Single-phase linear elastic	E = 15 MPa, ν = 0.475	40
Menisci	Isotropic material	E = 120 MPa, ν = 0.45	40
ACL	Neo-Hookean	C_1 = 1.95MPa, C_2 = 0 MPa, C_3 = 0.0139 MPa, C_4 = 116.22 MPa, C_5 = 535.039 MPa, λ^* = 1.046, D = 0.00683 MPa^{-1}	42
PCL		C_1 = 2.75MPa, C_2 = 0 MPa, C_3 = 0.065 MPa, C_4 = 115.89 MPa, C_5 = 512.73 MPa, λ^* = 1.042 MPa, D = 0.00484 MPa^{-1}	42
MCL/LCL		C_1 = 1.44MPa, C_2 = 0 MPa, C_3 = 0.57 MPa, C_4 = 48.0 MPa, C_5 = 467.1 MPa, λ^* = 1.063 MPa, a D = 0.00126 MPa^{-1}	42

Table 1. Material parameters of each knee component. *ACL* anterior cruciate ligament, *PCL* posterior cruciate ligament, *LCL* lateral collateral ligament, *MCL* medial collateral ligament, *E* elastic modulus, *v* Poisson ratio.

$$\psi = \psi_{iso} + \psi_{aniso} + \psi_{v}$$

The ligament matrix was modeled as a hyperelastic Neo-Hookean material[41,42], with the strain energy function defined as $\psi_{iso} = C_1\left(\bar{I}_1 - 3\right)$, where C_1 is the material constant and $\bar{I}_1$ is the first invariant of the right Cauchy–Green tensor. The collagen fibers of the ligaments were designed to support only tensile forces. The nonlinear relationship between the tensile force and the tensile strain of the fibers was expressed as follows:

$$\lambda \frac{\partial \psi_{aniso}}{\partial \lambda} = \begin{cases} 0 & , \lambda < 1 \\ C_3\left(e^{C_4(\lambda-1)}-1\right) & , 1 \le \lambda \le \lambda^* \\ C_5\lambda + C_6 & , \lambda > \lambda^* \end{cases}$$

where C_3 、 C_4 、 C_5 and λ^* are material constants, and the incompressible volume of the ligament is expressed as: $\psi_v = \frac{1}{D}[ln(J)]^2$. Reciprocal bulk modulus at the D position. J is the Jacobian of the movement, and F denotes the deformation gradient, $J = detF$. These models and material properties were defined based on relevant data and parameters from scientific literature to ensure the accuracy and reliability of the FEA. The material coefficients are presented in Table 1.

Boundary conditions and loading

After assembling the model and assigning materials to its components in ANSYS Workbench, six contact pairs (medial knee compartment: femoral cartilage-medial meniscus, medial meniscus-tibial medial cartilage, and femoral cartilage-tibial medial cartilage; lateral knee compartment: femoral cartilage-lateral meniscus, lateral meniscus-tibial lateral cartilage, and femoral cartilage-tibial lateral cartilage) in the medial and lateral knee compartments were defined as sliding friction contacts with a friction coefficient of μ = 0.002 [43]. This setup ensured that there was no penetration and limited sliding between contact pairs. To investigate the biomechanical relationships within the knee joint, this study fixed the three degrees (X-axis, Y-axis, and Z-axis) of freedom at the distal ankle joint center of the tibia and fibula. A force of 1000 N was applied along the Z-axis (mechanical axis) at the center of the femoral head while constraining the other two degrees (X-axis and Y-axis) of freedom at the femoral head center[44,45]. This simulation was designed to replicate knee joint biomechanics during conditions similar to the stance phase.

Convergence testing and model sizing

Based on the boundary conditions and material parameters set in this study, these conditions were applied to the model. The present study conducted mesh convergence tests on the displacement of the medial and lateral menisci. The mesh size for the knee joint cartilage (femoral cartilage, medial tibial cartilage, lateral tibial cartilage), menisci (medial and lateral), and ligaments (ACL, PCL, MCL, and LCL) were refined relative to the mesh size at the bone surfaces. The mesh size for the soft tissue surfaces of the knee joint decreased progressively from 2.0 mm to 0.5 mm, whereas the surface mesh size for other parts of the bone model was maintained at 3.0 mm.

In this study model, mesh convergence was tested using element edge lengths ranging from 2.0 to 0.5 mm. When the element edge length varied between 2.0 and 0.8 mm, the maximum difference in displacement values for the MM from the mean of the obtained results was approximately 38.5%. Reducing the element edge length further, from 0.8 to 0.5 mm, decreased the maximum difference in displacement values to 4.0%. While further reductions in edge length may result in even smaller differences, the present study selected a relatively fine mesh with an edge length of 0.8 mm for the soft tissue surfaces of the knee joint. Once the surface mesh was defined, a volume mesh was generated using the C3D10 tetrahedral elements. After assembling 21 models, the average number of nodes was approximately 1,752,412 and the average number of elements was approximately 3,570,118.

Data availability

The datasets generated during and/or analysed during the current study are available from the corresponding author on reasonable request.

Received: 22 November 2024; Accepted: 18 March 2025
Published online: 23 March 2025

References

1. Hwang, B. Y. et al. Risk factors for medial meniscus posterior root tear. *Am. J. Sports Med.* **40**, 1606–1610. https://doi.org/10.1177/0363546512447792 (2012).
2. Ozkoc, G. et al. Radial tears in the root of the posterior Horn of the medial meniscus. *Knee Surg. Sports Traumatol. Arthrosc.* **16**, 849–854. https://doi.org/10.1007/s00167-008-0569-z (2008).
3. Marzo, J. M. & Gurske-DePerio, J. Effects of medial meniscus posterior Horn avulsion and repair on tibiofemoral contact area and peak contact pressure with clinical implications. *Am. J. Sports Med.* **37**, 124–129. https://doi.org/10.1177/0363546508323254 (2009).
4. Kodama, Y. et al. Transtibial fixation for medial meniscus posterior root tear reduces posterior extrusion and physiological translation of the medial meniscus in middle-aged and elderly patients. *Knee Surg. Sports Traumatol. Arthrosc.* **28**, 3416–3425. https://doi.org/10.1007/s00167-019-05810-x (2020).
5. Padalecki, J. R. et al. Biomechanical consequences of a complete radial tear adjacent to the medial meniscus posterior root attachment site: in situ pull-out repair restores derangement of joint mechanics. *Am. J. Sports Med.* **42**, 699–707. https://doi.org/10.1177/0363546513499314 (2014).
6. Bernard, C. D. et al. Medial meniscus posterior root tear treatment: A matched cohort comparison of nonoperative management, partial meniscectomy, and repair. *Am. J. Sports Med.* **48**, 128–132. https://doi.org/10.1177/0363546519888212 (2020).
7. Dong, T. et al. Radiographic measures of settlement phenomenon in patients with medial compartment knee osteoarthritis. *Clin. Rheumatol.* **35**, 1573–1578. https://doi.org/10.1007/s10067-015-3146-0 (2016).
8. Chambers, C. C., Lynch, J. A., Feeley, B. T. & Nevitt, M. C. Association of medial meniscus root tears and nonroot tears with worsening of radiographic knee osteoarthritis. *Orthop. J. Sports Med.* **11**, 23259671231195894. https://doi.org/10.1177/23259671231195894 (2023).
9. Moon, H. S. et al. Early surgical repair of medial meniscus posterior root tear minimizes the progression of meniscal extrusion: 2-Year Follow-up of clinical and radiographic parameters after arthroscopic transtibial Pull-out repair. *Am. J. Sports Med.* **48**, 2692–2702. https://doi.org/10.1177/0363546520940715 (2020).
10. Lan, M. et al. High tibial osteotomy with posterior medial meniscal root reconstruction yields improved radiographic and functional outcomes and healing rates compared to osteotomy alone. *Arthroscopy* https://doi.org/10.1016/j.arthro.2024.06.039 (2024).
11. Kim, C. W., Lee, C. R. & Son, G. H. Type of medial meniscus tear does not affect the clinical and radiological outcomes of medial opening-wedge high tibial osteotomy. *Knee Surg. Sports Traumatol. Arthrosc.* **31**, 5025–5033. https://doi.org/10.1007/s00167-023-07542-5 (2023).
12. Horita, K. et al. High tibial osteotomy alone does not decrease medial meniscus extrusion in the setting of medial meniscus posterior root tear: A cadaveric study. *Arthroscopy* https://doi.org/10.1016/j.arthro.2024.06.038 (2024).
13. Park, H. J. et al. Medial meniscus posterior root repair restores contact pressure and contact area to its native state even after Opening-Wedge high tibial osteotomy: A cadaveric Biomechanical study. *Arthroscopy* **39**, 638–646. https://doi.org/10.1016/j.arthro.2022.09.009 (2023).
14. Choi, Y. S. et al. Repair of medial meniscus posterior root tear is effective for root healing and cartilage regeneration in opening wedge high tibial osteotomy. *Knee Surg. Sports Traumatol. Arthrosc.* **31**, 5799–5811. https://doi.org/10.1007/s00167-023-07637-z (2023).
15. Jing, L. et al. Second-look arthroscopic findings after medial open-wedge high tibial osteotomy combined with all-inside repair of medial meniscus posterior root tears. *J. Orthop. Surg. (Hong Kong)*. **28**, 2309499019888836. https://doi.org/10.1177/2309499019888836 (2020).
16. Cheng, X., Liu, F., Xiong, F., Huang, Y. & Paulus, A. C. Radiographic changes and clinical outcomes after open and closed wedge high tibial osteotomy: a systematic review and meta-analysis. *J. Orthop. Surg. Res.* **14**, 179. https://doi.org/10.1186/s13018-019-1222-x (2019).
17. Ducat, A. et al. Posterior tibial slope changes after opening- and closing-wedge high tibial osteotomy: a comparative prospective multicenter study. *Orthop. Traumatol. Surg. Res.* **98**, 68–74. https://doi.org/10.1016/j.otsr.2011.08.013 (2012).
18. Nha, K. W., Kim, H. J., Ahn, H. S. & Lee, D. H. Change in posterior tibial slope after Open-Wedge and Closed-Wedge high tibial osteotomy: A Meta-analysis. *Am. J. Sports Med.* **44**, 3006–3013. https://doi.org/10.1177/0363546515626172 (2016).
19. Okazaki, Y. et al. Steep posterior slope and shallow concave shape of the medial tibial plateau are risk factors for medial meniscus posterior root tears. *Knee Surg. Sports Traumatol. Arthrosc.* **29**, 44–50. https://doi.org/10.1007/s00167-019-05590-4 (2021).
20. Dzidzishvili, L. et al. Increased posterior tibial slope is associated with increased risk of meniscal root tears: A systematic review. *Am. J. Sports Med.* **3635465231225981** https://doi.org/10.1177/03635465231225981 (2024).
21. LaPrade, R. F., Oro, F. B., Ziegler, C. G., Wijdicks, C. A. & Walsh, M. P. Patellar height and tibial slope after opening-wedge proximal tibial osteotomy: a prospective study. *Am. J. Sports Med.* **38**, 160–170. https://doi.org/10.1177/0363546509342701 (2010).
22. Giffin, J. R., Vogrin, T. M., Zantop, T., Woo, S. L. & Harner, C. D. Effects of increasing tibial slope on the biomechanics of the knee. *Am. J. Sports Med.* **32**, 376–382. https://doi.org/10.1177/0363546503258880 (2004).
23. Omae, H. et al. Arthroscopic pullout repair versus suture anchor repair for medial meniscus posterior root tear combined with high tibial osteotomy. *Knee* **45**, 117–127. https://doi.org/10.1016/j.knee.2023.10.011 (2023).
24. Hiranaka, T. et al. Steep medial tibial slope and prolonged delay to surgery are associated with bilateral medial meniscus posterior root tear. *Knee Surg. Sports Traumatol. Arthrosc.* **29**, 1052–1057. https://doi.org/10.1007/s00167-020-06079-1 (2021).
25. Nakamura, R., Kuroda, K., Takahashi, M. & Katsuki, Y. Open wedge high tibial osteotomy with Pes Anserinus preservation and insertion of bone substitutes. *Arthrosc. Tech.* **11**, e69–e78. https://doi.org/10.1016/j.eats.2021.09.002 (2022).
26. Ogawa, H., Matsumoto, K., Ogawa, T., Takeuchi, K. & Akiyama, H. Effect of wedge insertion angle on posterior tibial slope in medial opening wedge high tibial osteotomy. *Orthop. J. Sports Med.* **4**, 2325967116630748. https://doi.org/10.1177/2325967116630748 (2016).
27. Kim, J. S. et al. Is there any benefit in the combined ligament reconstruction with osteotomy compared to ligament reconstruction or osteotomy alone? Comparative outcome analysis according to the degree of medial compartment osteoarthritis with anterior or posterior cruciate ligament insufficiency. *Arch. Orthop. Trauma. Surg.* **143**, 3677–3689. https://doi.org/10.1007/s00402-022-04544-9 (2023).
28. Teng, Y. et al. Axial but not sagittal hinge axis affects posterior tibial slope in medial Open-Wedge high tibial osteotomy: A 3-Dimensional surgical simulation study. *Arthroscopy* **37**, 2191–2201. https://doi.org/10.1016/j.arthro.2021.01.063 (2021).
29. Tollefson, L. V., Lee, D., Keel, T., LaPrade, C. M. & LaPrade, R. F. Medial opening wedge (MOW) versus lateral closing wedge (LCW) high tibial osteotomies for knee medial compartment osteoarthritis show similar outcomes and survivorship, while MOW has higher rates of tibial fracture and LCW has higher rates of nerve injury and conversion to total knee. *Arthroscopy* https://doi.org/10.1016/j.arthro.2024.11.002 (2024).
30. Yokoe, T. et al. Shear stress in the medial meniscus posterior root during daily activities. *Knee* **43**, 176–183. https://doi.org/10.1016/j.knee.2023.06.008 (2023).

31. Fürmetz, J. et al. Three-dimensional assessment of lower limb alignment: accuracy and reliability. *Knee* **26**, 185–193. https://doi.org/10.1016/j.knee.2018.10.011 (2019).
32. Fujisawa, Y., Masuhara, K. & Shiomi, S. The effect of high tibial osteotomy on osteoarthritis of the knee. An arthroscopic study of 54 knee joints. *Orthop. Clin. North. Am.* **10**, 585–608 (1979).
33. Cobb, J. P., Dixon, H., Dandachli, W. & Iranpour, F. The anatomical tibial axis: reliable rotational orientation in knee replacement. *J. Bone Joint Surg. Br.* **90**, 1032–1038. https://doi.org/10.1302/0301-620x.90b8.19905 (2008).
34. Kang, K. T., Koh, Y. G., Lee, J. A., Lee, J. J. & Kwon, S. K. Biomechanical effect of a lateral hinge fracture for a medial opening wedge high tibial osteotomy: finite element study. *J. Orthop. Surg. Res.* **15**, 63. https://doi.org/10.1186/s13018-020-01597-7 (2020).
35. Jörgens, M. et al. Reliability of 3D planning and simulations of medial open wedge high tibial osteotomies. *J. Orthop. Surg. (Hong Kong)*. **30**, 10225536221101699. https://doi.org/10.1177/10225536221101699 (2022).
36. Dean, R. S., DePhillipo, N. N., Chahla, J., Larson, C. M. & LaPrade, R. F. Posterior tibial slope measurements using the anatomic axis are significantly increased compared with those that use the mechanical axis. *Arthroscopy* **37**, 243–249. https://doi.org/10.1016/j.arthro.2020.09.006 (2021).
37. Petersen, W. et al. Posterior root tear of the medial and lateral meniscus. *Arch. Orthop. Trauma. Surg.* **134**, 237–255. https://doi.org/10.1007/s00402-013-1873-8 (2014).
38. Kamatsuki, Y. et al. Accurate placement of a tibial tunnel significantly improves meniscal healing and clinical outcomes at 1 year after medial meniscus posterior root repair. *Knee Surg. Sports Traumatol. Arthrosc.* **29**, 3715–3723. https://doi.org/10.1007/s00167-020-06376-9 (2021).
39. Steineman, B. D., LaPrade, R. F. & Haut Donahue, T. L. Nonanatomic placement of posteromedial meniscal root repairs: A finite element study. *J. Biomech. Eng.* **142** https://doi.org/10.1115/1.4045893 (2020).
40. Li, L. et al. Three-dimensional finite-element analysis of aggravating medial meniscus tears on knee osteoarthritis. *J. Orthop. Translat*. **20**, 47–55. https://doi.org/10.1016/j.jot.2019.06.007 (2020).
41. Weiss, J. A., Maker, B. N. & Govindjee, S. Finite element implementation of incompressible, transversely isotropic hyperelasticity. *Comput. Methods Appl. Mech. Eng.* **135**, 107–128. https://doi.org/10.1016/0045-7825(96)01035-3 (1996).
42. Pena, E., Martinez, M. A., Calvo, B., Palanca, D. & Doblare, M. A finite element simulation of the effect of graft stiffness and graft tensioning in ACL reconstruction. *Clin. Biomech. (Bristol Avon)*. **20**, 636–644. https://doi.org/10.1016/j.clinbiomech.2004.07.014 (2005).
43. Xu, Z. et al. Biomechanical assessment of disease outcome in surgical interventions for medial meniscal posterior root tears: a finite element analysis. *BMC Musculoskelet. Disord.* **23**, 1093. https://doi.org/10.1186/s12891-022-06069-z (2022).
44. Luczkiewicz, P. et al. The influence of a change in the meniscus cross-sectional shape on the medio-lateral translation of the knee joint and meniscal extrusion. *PLoS One*. **13**, e0193020. https://doi.org/10.1371/journal.pone.0193020 (2018).
45. Bao, H. R., Zhu, D., Gong, H. & Gu, G. S. The effect of complete radial lateral meniscus posterior root tear on the knee contact mechanics: a finite element analysis. *J. Orthop. Sci.* **18**, 256–263. https://doi.org/10.1007/s00776-012-0334-5 (2013).

Acknowledgements

We thank Mr. Takashi Nakamura and Mr. Masahiro Enzaki for their contributions to the CT and MRI scanning.

Author contributions

Conception and design of study: Fan Yang, Takuji Yokoe. acquisition of data: Fan Yang, Koki Ouchi. analysis and/or interpretation of data: Fan Yang, Takuji Yokoe, Koki Ouchi. Drafting the manuscript: Fan Yang, Takuji Yokoe. revising the manuscript critically for important intellectual content: Takuya Tajima, Naosuke Kamei, Etsuo Chosa. All authors have read and approved the final manuscript.

Declarations

Competing interests

The authors declare no competing interests.

Additional information

Correspondence and requests for materials should be addressed to T.Y.